1. AGENCY USE ONLY (Leave Blank)	2. REPORT DATE	3. REPORT TYPE AND DATES COVERED
	06/01/01	Final ~~10/01/98~~ 01 Apr 98 - 03/31/01

4. TITLE AND SUBTITLE	5. FUNDING NUMBERS
Synthesis and Characterization of Rare Earth Doped Wide Bandgap Materials	G ARO-DAAG55-98-1-0216 ARO-DAAG55-98-1-0216
6. AUTHOR(S) Cammy R. Abernathy	
7. PERFORMING ORGANIZATION NAME(S) AND ADDRESS(ES) University of Florida Gainesville, Florida 32611	8. PERFORMING ORGANIZATION REPORT NUMBER
9. SPONSORING / MONITORING AGENCY NAME(S) AND ADDRESS(ES) U. S. Army Research Office P.O. Box 12211 Research Triangle Park, NC 27709-2211	10. SPONSORING / MONITORING AGENCY REPORT NUMBER 35730.6-EL

11. SUPPLEMENTARY NOTES

The views, opinions and/or findings contained in this report are those of the author(s) and should not be construed as an official Department of the Army position, policy or decision, unless so designated by other documentation.

12 a. DISTRIBUTION / AVAILABILITY STATEMENT	12 b. DISTRIBUTION CODE
Approved for public release; distribution unlimited.	

13. ABSTRACT (Maximum 200 words)

INTRODUCTION

It has been found that codopant impurities (O, C, F) can enhance the luminescence and efficiency of Si:Er [1-5], but only when introduced in the proper Er/Impurity ratio. While it has been shown that addition of elements such as C and O can enhance the IR emission from GaN:Er [6], there has as yet been no systematic investigation of the role of the concentration of these codopants in the luminescence and surface properties of the GaN films. In this work, the effect of C codoping introduced via CBr_4 on the structural and optical properties of GaN:Er films grown on sapphire by gas source molecular beam epitaxy (GSMBE) has been investigated in an attempt to address these issues. The effect of post-growth annealing on PL intensity in the carbon-doped material has also been explored. Finally, Eu-doping of GaN has been investigated for potential use in red emitting devices.

14. SUBJECT TERMS	15. NUMBER OF PAGES
Rare Earth Doped Wide Bandgap Materials	24
	16. PRICE CODE

17. SECURITY CLASSIFICATION OR REPORT	18. SECURITY CLASSIFICATION ON THIS PAGE	19. SECURITY CLASSIFICATION OF ABSTRACT	20. LIMITATION OF ABSTRACT
UNCLASSIFIED	UNCLASSIFIED	UNCLASSIFIED	UL

SYNTHESIS AND CHARACTERIZATION OF RARE EARTH DOPED WIDE BANDGAP MATERIALS

Contract No. ARO- DAAG55-98-1-0216

FINAL REPORT

March 31, 2001

T.O.C. : **C. R. Abernathy**
Dept. of Materials Sci. and Eng.
University of Florida
Gainesville, FL 32606

1.0 INTRODUCTION

Under a previous AASERT grant from ARO (Contract No. DAAH04-95-1-0196), the incorporation behavior of Er from various sources was investigated. The Er sources explored in that study were erbiumtetramethylheptanedionate (ErTMHD), erbiumbistrimethylsilylamide (ErBTSiN) which has the chemical formula $Er\{N\{Si(CH_3)_3]_2\}_6$ and elemental Er. Post-growth secondary ion mass spectroscopy (SIMS) (performed by R. G. Wilson from Hughes Research Lab at Charles Evans and Assoc.) did not detect Er above the background detection limit of $\sim 10^{16}$ cm^{-3} in the samples doped using gaseous sources. The conclusion was therefore that the low vapor pressures and low incorporation efficiencies of these compounds make room temperature transport unfeasible. Elemental Er was used to dope AlN, GaN and InAlN on both sapphire and Si substrates during growth by metalorganic molecular beam epitaxy (MOMBE). The resulting Er concentrations obtained by this method were quite high. Most importantly, the PL signal obtained from this material was found to be quite intense, and in fact, represented the highest room temperature signal obtained to date from Er-doped nitrides.

Building upon this work, the optical and electrical excitation of Er^{3+} in III-N materials and in device structures on Si has been investigated under this program. Luminescence (PL: UF and Uwe Hommerich at Hampton Univ., CL: L. Brillson at Ohio State Univ.), implantation (R. G. Wilson), lifetime (U. Hommerich) and annealing experiments to further elucidate the optical excitation mechanisms in MOMBE-derived GaN:Er have been performed on materials with varying concentrations of Er and co-dopants such as oxygen and carbon. These mechanisms have then been compared to Er excitation models proposed in other semiconductor:Er systems. In addition, room-temperature electroluminescence (EL) from simple metal/GaN:Er/Si and metal/InAlN:Er/Si structures has been demonstrated (testing by P. Shen at ARL).

In addition to Er, Eu was also investigated. While the III-Nitrides have proven quite successful for fabrication of blue and green light emitting devices, realization of red devices has not been successful due to the difficulties associated with the synthesis of the high In-content InGaN needed to achieve red emission. An attractive alternative may be the use of Eu-doped GaN, whose emission wavelength is host-material insensitive. The reduction in quenching which allows efficient operation of Er-doped material at room temperature should offer the same benefit for Eu^{+3}. In the past, Eu doping has been utilized to produce emission in organic-based devices[1], phosphor applications[2], and in CaF_2-based devices[3]. The use of red emitting GaN:Eu has also been previously reported[4,5]. However, the intensity of GaN:Eu has yet to be compared to materials used for commercially available LED devices. In this study, red emission from GaN doped with Eu was compared to the emission from high quality metalorganic chemical vapor deposition (MOCVD) derived AlGaAs. The luminescence and thermal quenching were also investigated before and after high temperature annealing.

2.0 RESULTS AND DISCUSSION

2.1 Effect of Er Concentration

In order to optimize the Er concentration, the effect of Er flux on material properties was investigated. Films were grown by MOMBE in an INTEVAC Gas Source Gen II on In-mounted (0001) Al_2O_3. A 20 nm low temperature AlN buffer layer (T_g = 435°C) preceded the GaN. Dimethylethylamine alane (DMEAA) and triethylgallium (TEGa) provided the group III fluxes.

Reactive nitrogen for the growth of both the AlN and the GaN was provided by an SVT RF plasma source operating at 375 W of forward power and 3 sccm of N_2. A shuttered effusion oven charged with 4 N Er was used for doping, with cell temperatures varying from 1250 – 1450°C. Previous calibration of this cell indicates an approximate concentration range of mid - 10^{18} to 10^{20} cm^{-3}, although SIMS analysis has not yet been performed to verify the concentrations in the samples used in this study. The GaN layer structures were grown at 750°C and consisted of ~500nm of undoped material followed by ~1.15 μm of Er doped material. Room temperature photoluminescence was used to evaluate the 1.54 μm emission. The Er^{+3} PL was excited using the 488 nm line of an Ar ion laser and measured with an InGaAs photodetector. The surface morphology was characterized by atomic force microscopy (AFM) using a Digital Instruments Nanoscope III and by scanning electron microscopy (SEM) using a JEOL 35CF .

The surface morphologies of the GaN:Er samples are shown in Figure 1 as a function of Er cell temperature. As the Er temperature, and therefore the Er concentration, was increased, the round surface features decreased in size until a smooth morphology was obtained at 1450°C. This is in sharp contrast to the result obtained from similar experiments with AlN. In AlN, as the Er concentration was increased, the surface roughness increased due to the formation of surface nodules. SIMS analysis of the AlN did not show any evidence of Er segregation and the nodules appeared to be of the same composition as the underlying matrix. It is possible that the Er, though not segregating, was clustering and thus disturbing the growth front. The fact that this degradation does not occur in GaN may suggest that the Er is more soluble due to the larger Group III site in GaN relative to AlN. It is surprising, however, that the GaN surface morphology actually improves with increasing Er content. From the SEM data it would appear that the surface is smoother due to a reduction in the domain size. GaN grown by MBE often

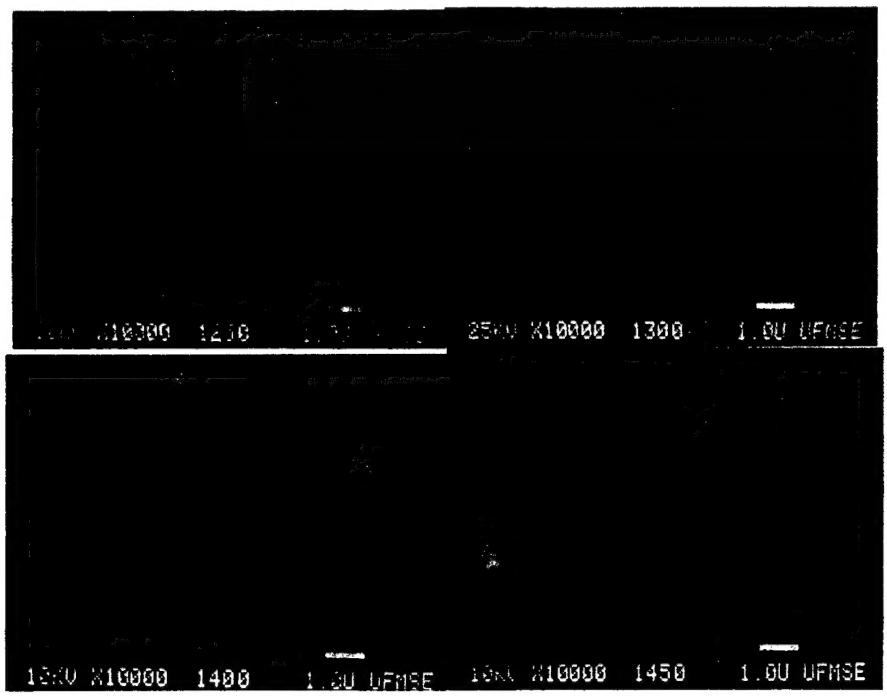

Figure 1: Scanning electron micrographs of GaN with a progression of Er cell temperatures: 1250°C (upper left), 1300°C (upper right), 1400°C (lower left) and 1450°C (lower right).

exhibits a columnar structure which is induced by the large lattice mismatch between the GaN and the sapphire. This reduction in column diameter is also supported by AFM measurements of the surface roughness, shown in Figure 2. The RMS roughness of the films decreased by an order of magnitude (from 18.1 nm to 2.0 nms) as the Er cell temperature was increased from 1250°C and 1450°C. When the AFM scans of the surface are examined in detail, seen in Figure 3, it is clear that the surface features are reduced in size. These results suggest that the Er may interfere with the surface migration of the reactant species resulting in a smoother less textured surface. This reduction in surface mobility also results in a slight decrease in the growth rate at high Er fluxes, as shown in Figure 4, probably due to enhanced desorption of the ethyl-gallium species.

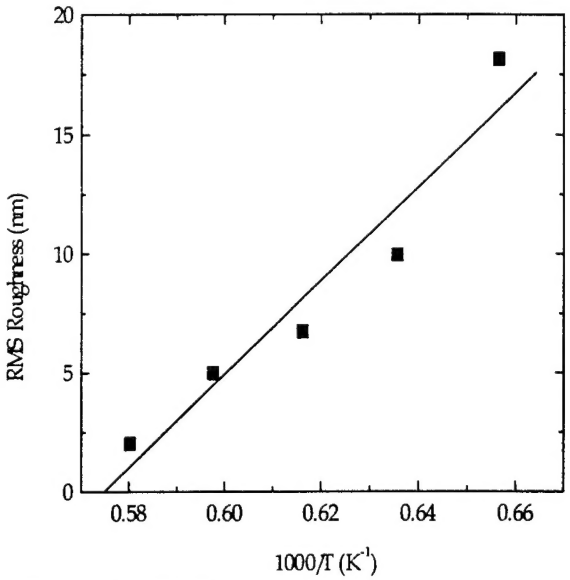

Figure 2: RMS roughness versus reciprocal Er cell temperature.

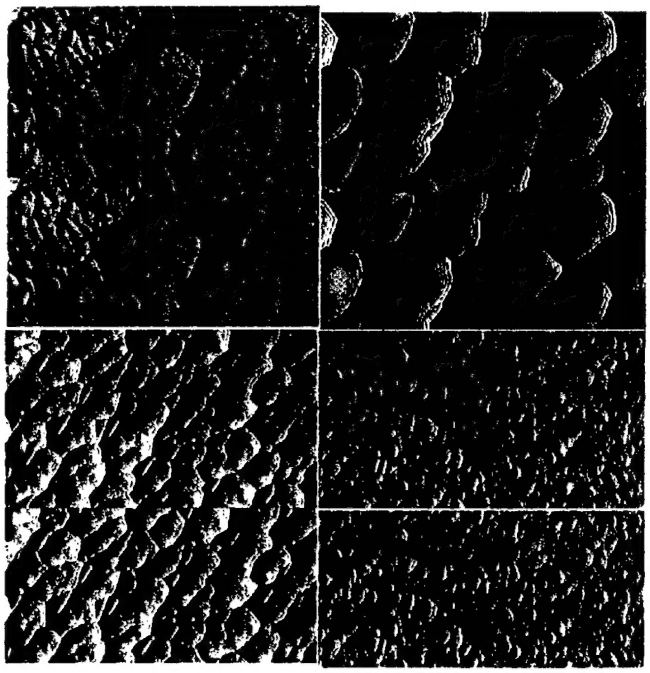

Figure 3: AFM surface scans of GaN with a progression of Er cell temperatures from: 1250°C (upper left), 1300°C (upper right), 1400°C (lower left) and 1450°C (lower right). Area represented is 1 μm x 1μm.

As hoped, PL analysis, depicted in Figure 5, shows that the normalized PL intensity increases steadily with increasing Er content, and shows no evidence of concentration quenching over the range investigated. The luminescence was fitted to an Arrenhius-type model and found to have a thermal activation energy of approximately 3.37 eV, which compares reasonably well to the activation energy for evaporation of Er in this same range of temperatures (~3.00 eV). This is roughly similar to the activation energy obtained from SIMS analysis of AlN:Er which was ~ 3.8 eV. Note that for AlN, however, the PL emission does not increase along with the Er concentration (see Figure 6). It is possible that due to the slightly larger radius of Ga compared to Al, it is more likely for Er^{+3} to sit on substitutional group III sites in the GaN lattice than in the AlN lattice. The greater ease of dopant incorporation in GaN:Er compared to AlN:Er would thus lead to more efficient optical activation and hence much greater PL signal at 1.54 μm. This enhanced substitutionality would also be in agreement with the smoother surface morphologies obtained in GaN relative to AlN. It is also possible that the saturation of the AlN:Er PL may be simply due to the degradation of the AlN crystal quality resulting from the poor incorporation behavior of Er in this material.

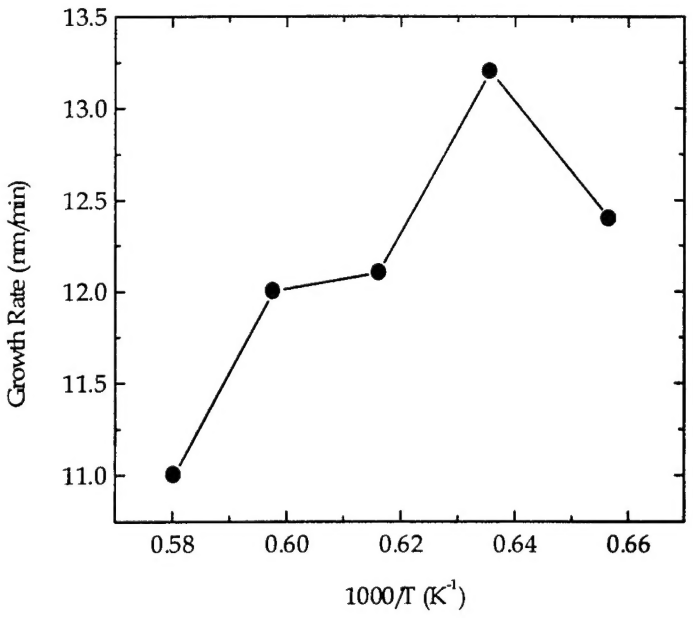

Figure 4. Growth rate of GaN:Er as a function of reciprocal Er cell temperature.

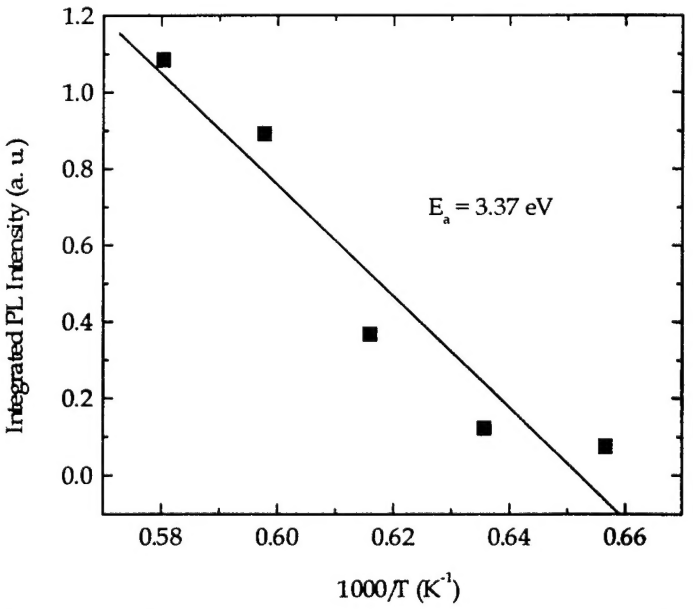

Figure 5: Integrated room temperature 1.54 μm PL for GaN:Er versus reciprocal Er cell temperature.

2.2 Effect of Co-Dopants

The surface morphologies of the GaN:Er samples codoped with different C levels from the CBr_4 source are shown in Figure 7. SEM micrograph A shows the undoped GaN surface. In micrographs B through D, as the CBr_4 flow, and therefore the C concentration, is increased, the round surface features decrease in size until a smooth morphology was obtained in GaN:Er that was codoped with roughly 1.3 x $10^{20}/cm^3$ of C. Upon further codoping, shown in micrograph E, it would appear that the round surface features then increase in size. The highest codopant level, shown in micrograph F, then appears to decrease in size again. The C concentration in micrograph F was approximately 1.3 x $10^{21}/cm^3$. From the SEM data, it would appear that the initial increase in film smoothness is due to a reduction in the GaN domain size. GaN grown by MBE often exhibits a columnar structure that is induced by the large lattice mismatch between the GaN and the sapphire.

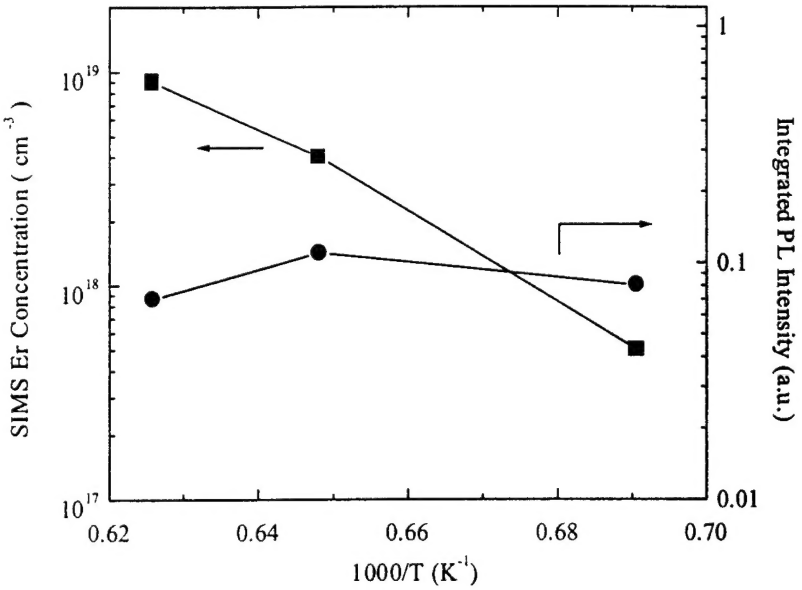

Figure 6: Er concentration as determined by SIMS and 1.54μm PL intensity for AlN versus reciprocal Er cell temperature.

As with the SEM, AFM measurements of the GaN:Er surface roughness indicate an initial improvement in morphology with increasing C level, as shown in Figure 7. The RMS surface roughness of the undoped GaN film was found to be approximately 73.5 Å. Upon the addition of Er, and with subsequent C addition, the surface roughness initially decreased by a factor of 7. However, with further C addition, the surface roughness increased dramatically. It is possible that at this C concentration (~$6x10^{20}/cm^3$), the GaN has reached its solubility limit. The increase in surface roughness could then be due to the incorporation of C in the form of defects, clusters, or precipitates. High levels of crystal defects were observed in Si:Er when the material system was "overdoped" with O [6]. With further C addition, the surface roughness drops for a CBr_4 flow of roughly 0.16 sccm. As shown in the AFM in Figure 9, rough regions and very smooth regions characterize this sample. The solid line in Figure 8 represents the overall surface roughness of the whole sample, while the dotted line represents the surface roughness of the smooth regions only. Note that there is roughly an order of magnitude drop between the two values. This suggests that coarsening effects due to increased C incorporation are opposed by surface etching of the GaN by Br left over from the CBr_4 decomposition.

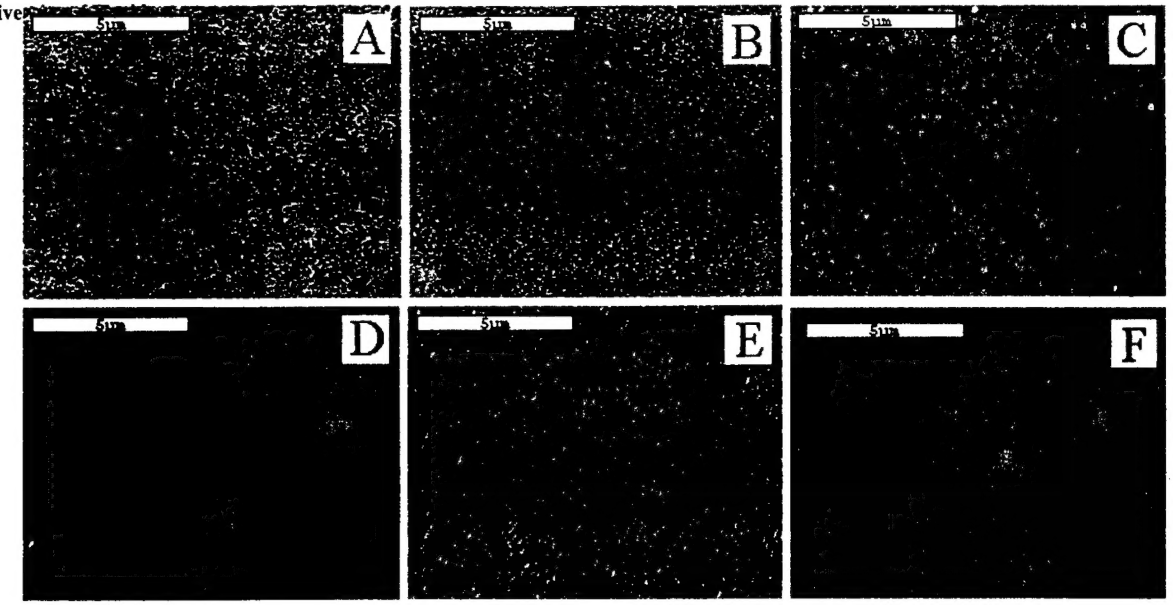

Fig. 7: SEMs of GaN and GaN:Er with a progression of CBr_4 doping (CBr_4 in sccm): (A) GaN, (B) GaN:Er, (C) GaN:Er (CBr_4=3.2x10^{-3}), (D) GaN:Er (CBr_4=1.6x10^{-2}), (E) GaN:Er (CBr_4=7.9x10^{-2}), and (F) GaN:Er (CBr_4=1.6x10^{-1}).

When the AFM surface scans, given in Figure 9, are examined in detail, it appears that the growth mode is altered for samples A through D. These results suggest that first the Er, then the C, may interfere with the surface migration of the reactant species, resulting in a smoother, less textured surface. The obvious roughening in micrograph E gives further credence to the theory that the GaN has reached its solubility limit for C, and that the roughening is due to an enhanced number of defects. Finally, in micrograph F, the defect related roughening is partially compensated by Br assisted surface etching.

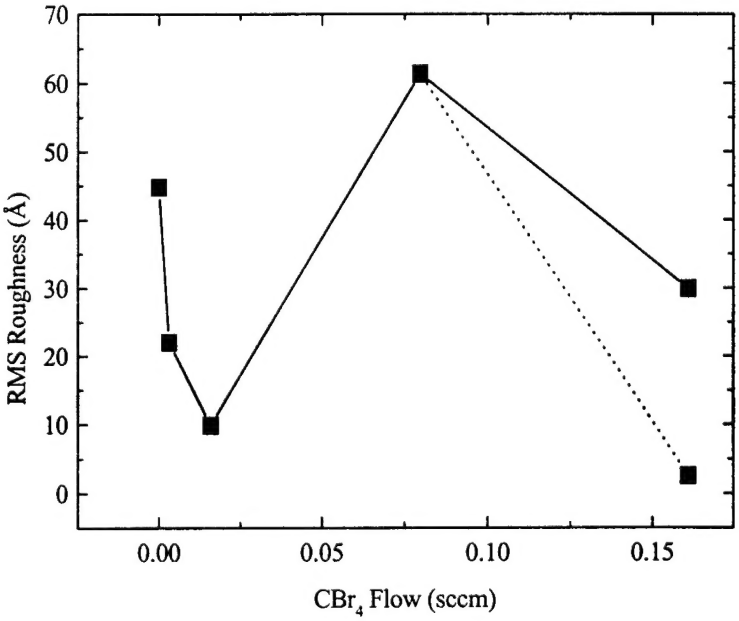

Fig. 8: GaN:Er RMS roughness vs. CBr_4 flux.

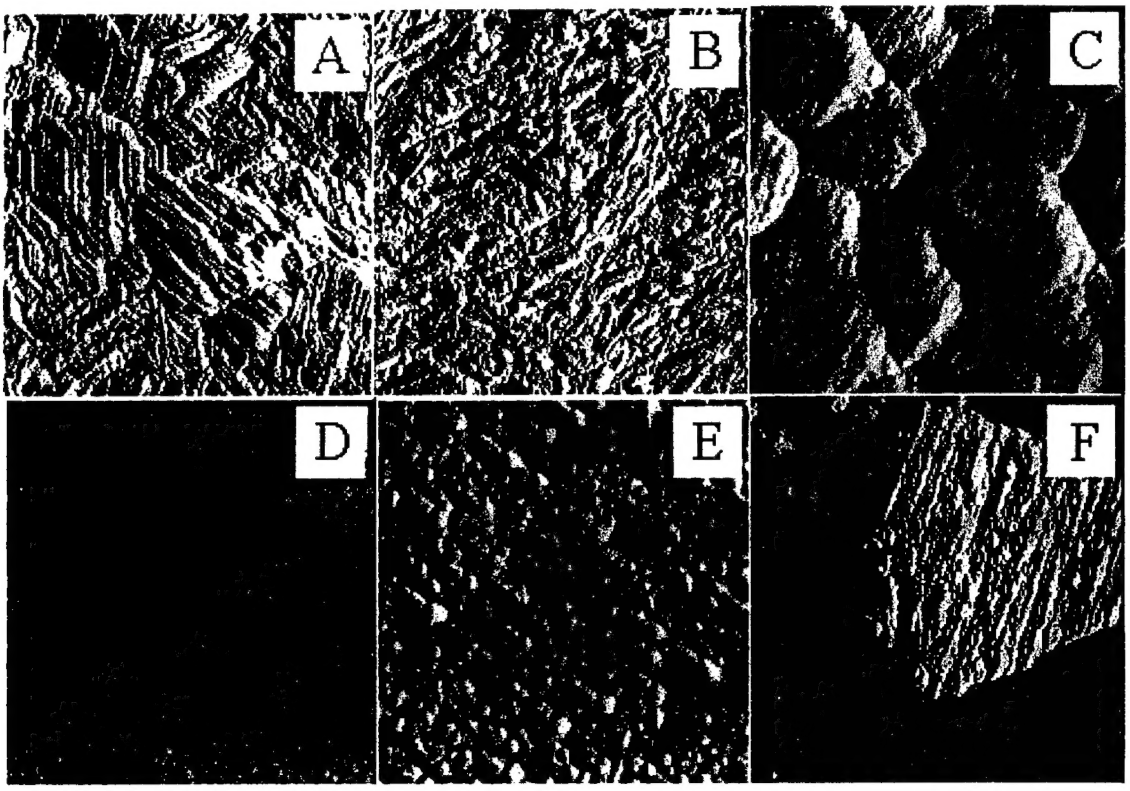

Fig. 9: AFM surface scans of GaN with a progression of Er and C doping (CBr_4 flux in sccm): (A) GaN, (B) GaN:Er, (C) GaN:Er (CBr_4=3.15x10^{-3}), (D) GaN:Er (CBr_4=1.6x10^{-2}), (E) GaN:Er (CBr_4=7.97x10^{-2}), and (F) GaN:Er (CBr_4=1.6x10^{-1}). Scan dimensions were 1 μm x 1 μm x 5 nm.

Figure 10 shows that the growth rate of the GaN: Er at first increases slightly with C incorporation, but then decreases as more C is added. The decrease in the growth rate at higher CBr_4 fluxes is almost certainly due to the Br species left over from the thermal decomposition of the CBr_4 at the growth surface which parasitically etches the GaN. Enhanced Br levels (and etch rates) due to the higher C fluxes will produce lower overall growth rates for the same initial GaN growth rate. Similar behavior has been observed in GaAs, GaP and AlGaAs.

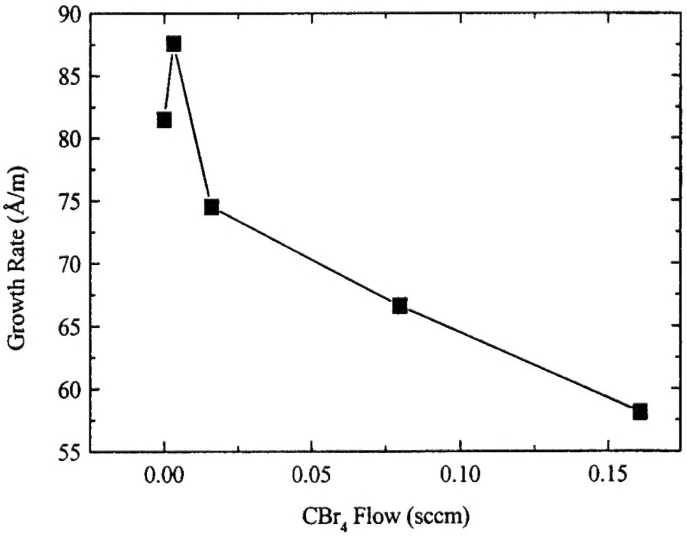

Fig. 10: GaN:Er growth rate vs. CBr_4 flux.

The PL analysis, depicted in Figures 11 and 12, shows that the PL intensity at first increases sharply with increased C content (over the non C-doped sample), and then decreases. This result indicates that for the Er concentration used (8.5 x $10^{20}/cm^3$), the optimum codoping concentration of C is ~7.7 x $10^{20}/cm^3$ as measured by SIMS. The initial increase in PL can be attributed to C affecting the local environment of the Er atoms. Normally, electric dipole radiation from 4f Er^{+3} transitions would be forbidden due to the parity selection rule. It has been found that a noncentrosymmetric crystal field leads to parity intermixing, resulting in a finite lifetime for radiative decay; such a crystal field can be produced by the formation of Er-C complexes, allowing efficient Er^{+3} pumping. It has also been suggested that a reduction in deep levels in the GaN, as well as enhanced promotion of Er from the +2 state to the +3 state by Er-C centers will produce a luminescence enhancement [7,8]. The decrease in the PL luminescence at high CBr_4 flows can be attributed to the further increased number of C atoms surrounding the Er producing nonradiative decay centers in the GaN matrix material. The nonradiative sites could be produced as a result of C-C clustering, precipitates, C related defects, and C atoms not linked to Er atoms. Similar results (optimum codopant level, enhanced nonradiative decay) have been seen previously in work done with Si:Er codoped with O [9,10].

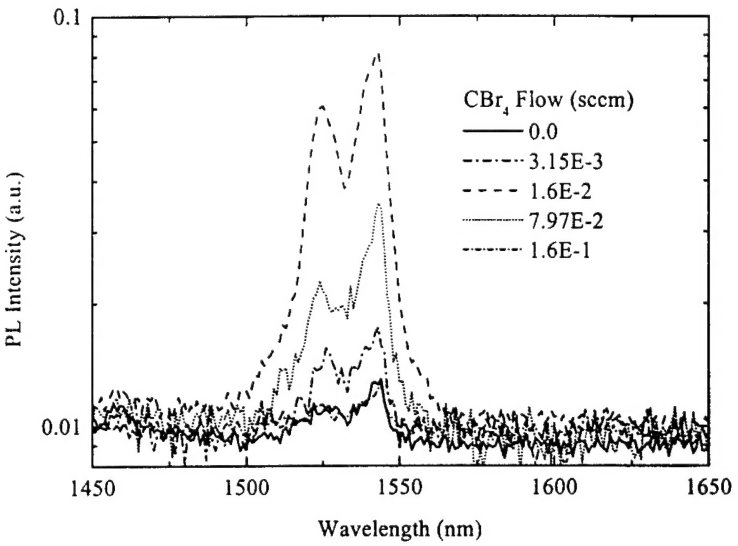

Fig. 11. Room temperature PL spectra taken from GaN:Er doped with carbon.

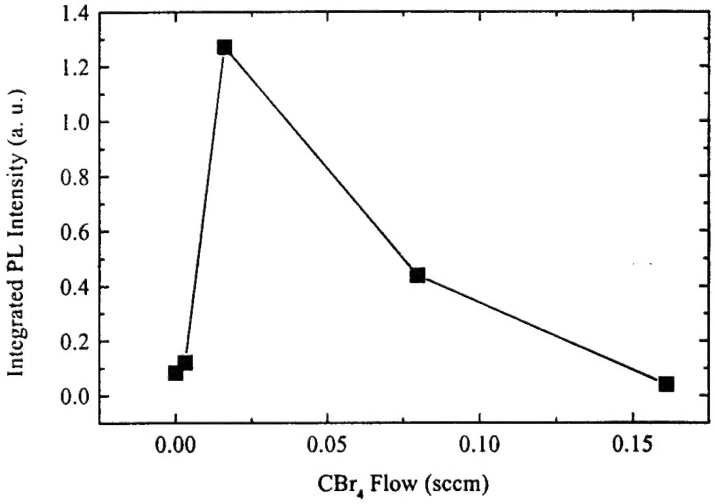

Fig. 12: Integrated PL intensity of the Er^{+3} emission at 1.54μm vs. CBr_4 flow.

The quenching behaviour of the carbon-doped material has also been investigated, shown in Figure 13. It was found that reducing the measurement temperature for the sample with the optimum carbon level produced a sharp increase in the peak located near 1535 nm, but not for the peak located near 1510. Comparison of the integrated intensity at 20K with that at 300K shows the thermal quenching to be ~40%. This is significantly higher than the degree of quenching observed for material grown with TEG, as shown in Table I, but much lower than is typically seen for low impurity GaN:Er which shows ~75% quenching. The material grown with

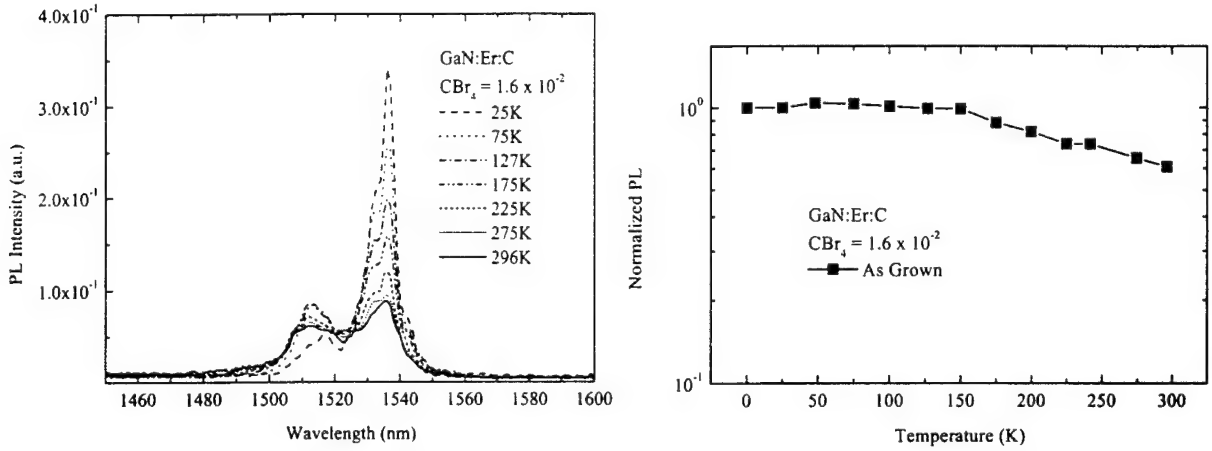

Fig. 13. PL emission vs. measurement temperature for GaN:Er,C.

TEG which contains an O/Er ratio of 0.9 in fact gave a higher integrated intensity at room temperature than at 20K. As shown in Figure 14, this negative quenching was due primarily to an increase in the secondary peak at 1510 as the main peak at 1535 remained virtually unchanged with temperature. Increasing the carbon concentration in the CBr_4 doped material did further suppress the quenching, though at the expense of the absolute emission. The oxygen levels in the samples grown with elemental Ga could not be determined due to a high oxygen background in the SIMS instrument. At the most, the oxygen level is ~3.5 x 10^{20} cm^{-3}. However, previous analysis of similarly grown material showed oxygen levels of ~10^{19} cm^{-3} or less. If similar levels are present in this material then the O/Er ratio would be ~0.01, which is significantly less than that obtained with TEG. Given that the C/Er ratios in the TEG grown material are the same or lower than those doped with CBr_4, it would appear that the reduced quenching in material grown with TEG is due to the presence of oxygen. TEG is synthesized with ether which can be transported to the growth surface, decompose and lead to high backgrounds of oxygen. It is most likely this oxygen which is responsible for the lack of thermal quenching.

Table 1: Impurity ratios and thermal quenching for GaN:Er grown using various sources along with an N_2 plasma.

Sources Used for Growth	[Er] (cm^{-3})	O/Er	C/Er	PL Intensity at 20K	Quenching Between 20K and 300K (%)
TEG	10^{22}	0.175	0.0084	0.9	0
TEG	10^{21}	0.9	2.3	1.7	-62%
Ga, CBr_4	$8.5x10^{20}$	< 0.4	9.0	1.4	31
Ga, CBr_4	$8.5x10^{20}$	< 0.4	0.9	4.0	40
Ga	$8.5x10^{20}$	< 0.4	-		75

From these results it would appear that oxygen is a better co-dopant for GaN:Er than carbon. Further, carbon produces mid-gap states which cause the material to be highly resistive. This could lead to high series resistance in actual devices. Oxygen, by contrast, behaves as a shallow donor, making the material conductive and possibly easier to fabricate into an efficient

device. Unfortunately the use of oxygen in UHV growth chambers can lead to contamination of the system, resulting in oxygen contamination throughout the device structure. In order to take advantage of the benefits of oxygen without compromising system integrity, a low vapor pressure oxygen-containing source which decomposes efficiently at the growth surface is needed.

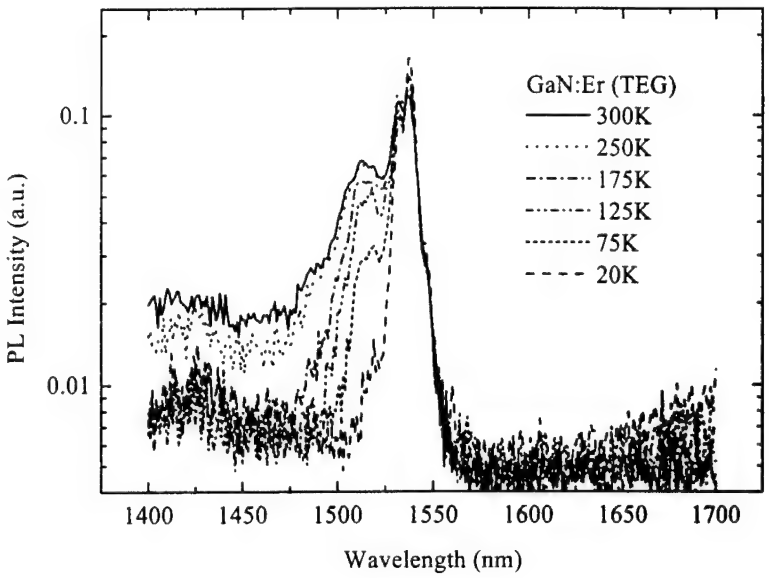

Fig. 14. PL spectra taken at various temperatures from GaN:Er grown using TEG with [Er] ~ $10^{21}cm^{-3}$.

2.3. Effect of Annealing

Annealing of the co-doped material produced no effect on the room temperature PL intensity for temperatures up to 600°C, regardless of ambient, as shown in Figure 15. Annealing at higher temperatures appeared to increase the intensity from carbon-doped material but did not increase the intensity from the GaN:Er without carbon. In fact, annealing in the forming gas ambient actually decreased the intensity from the non-carbon-doped material. This suggests that annealing enhances the Er-C interaction, and possibly helps to remove some of the defects generated by the introduction of high amounts of carbon.

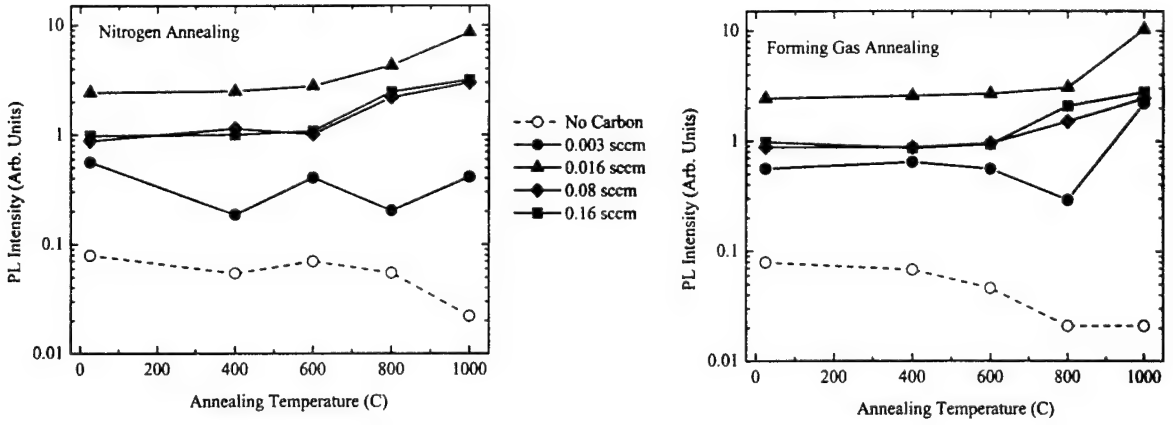

Fig. 15 Effect of annealing on room temperature 1.54μm PL intensity from GaN:Er using Ar^+ laser excitation. The annealing ambient was either nitrogen (at left) or forming gas (at right). The CBr_4 flows used during growth of the various layers are listed in the figure.

2.4 EL Structures

Electroluminescent structures were fabricated from TEGa-derived GaN:Er films grown on p-type (001) Si. The film stack consisted of approximately 6000 Å of GaN solid source-doped with Er to a concentration of ~3 x 10^{18} cm^{-3}, a 2000 Å GaN spacer layer, and a low temperature AlN buffer as in Figure 16. Secondary ion mass spectrometry (SIMS) analysis indicated that the GaN films had carbon and oxygen concentrations of ~10^{21} cm^{-3} and ~10^{20} cm^{-3}, respectively. Metallized contacts were made to front and backside with the assistance of Dr. Fan Ren at Lucent Technologies in Murray Hill, New Jersey (now in the Department of Chemical Engineering, University of Florida). A cross-section diagram of the metal-GaN:Er-Si structure is shown in Figure 16. A scanning electron micrograph of the topside of the structures showing the patterned top-contact metallization is shown in Figure 17. Room-temperature electroluminescence (EL) was observed in this structure under high, reverse-bias (> 20V) conditions, demonstrating for the first time, near-infrared EL from GaN:Er grown directly on a Si substrate. A preliminary 1.54 μm-region EL spectra is shown in Figure 18.

Schottky and p/n diode structures were also fabricated from $In_{0.23}Al_{0.77}N$ (n-type) films. After annealing, EL was observed from the Schottky structure grown on n^+-Si in reverse bias. However, luminescence was not observed from devices fabricated from $In_{0.23}Al_{0.77}N$

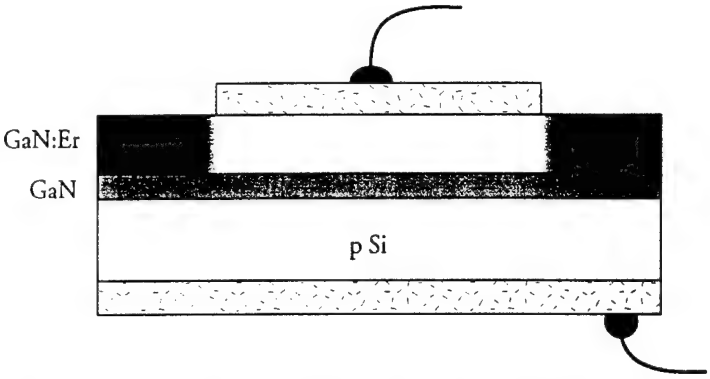

Figure 16. Cross-section diagram of the metal-GaN:Er-Si electroluminescent device structure.

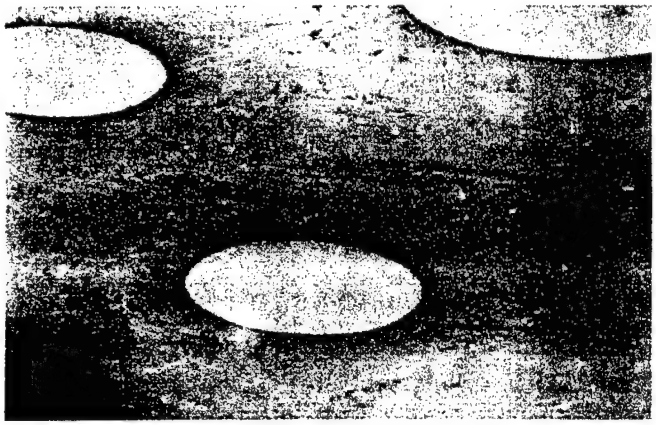

Figure 17. Scanning electron micrograph (600X) of the metallized surface of an LED-processed GaN:Er sample.

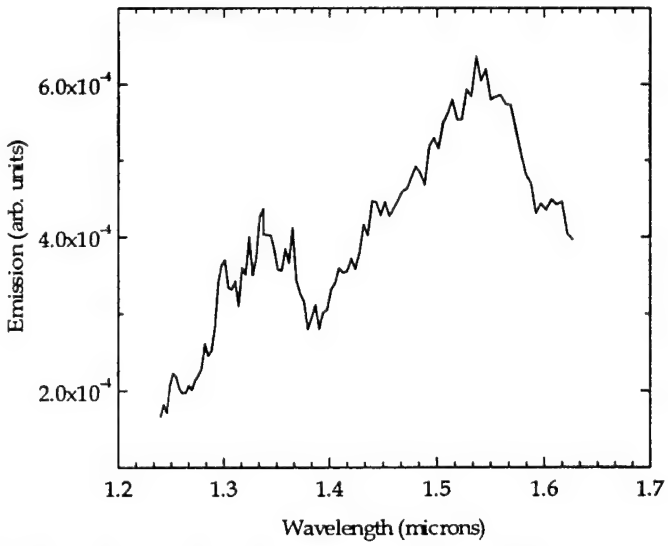

Figure 18. Room-temperature electroluminescence spectra of the GaN:Er device structure outlined in Figure 2-2. Spectra was taken at 20 V reverse bias.

deposited on p-GaAs. This is likley due to the fact that reverse bias breakdown in the $In_{0.23}Al_{0.77}N$/p-GaAs sample occurs first in the lower gap GaAs instead of in the Er-doped nitride.

The energy transfer mechanism causing emission in these devices is most likely impact excitation of Er or Er-complexes by electrons accelerated in the applied field. An estimation of the average transfer of energy from the applied electric field to the electron kinetic energy, assuming isotropic scattering, is given by: $(qE_{el}\lambda)^2/4E_p$,[11] where E_{el} is the electric field in the depletion region [~2.5 x 10^5 V/cm], (the entire GaN:Er + GaN film is assumed to be depleted); λ is the mean free path for optical phonon collisions [~5 nm], estimated from the value for Si; and E_p is the energy lost by optical phonon collisions, 73 meV[12]. This gives an electron kinetic energy on the order of 0.5 eV. Assuming a distribution of energies around that mean, a fraction of the accelerated electrons would have sufficient energy to excite the Er^{3+} ions (at least 0.8 eV). This is similar to electroluminescence observed in high oxygen-content semi-insulating polycrystalline Si (SIPOS) structures biased at 20 V as demonstrated by Lombardo et. al. [13] and in GaN:Er on Al_2O_3 devices formed by ion implantation.[14] Higher GaN:Er/Si device biases would likely result in higher Er^{3+} EL intensity as the average electron kinetic energy approaches the $^4I_{11/2}$ Er^{3+} pump level at approximately 1.2 eV as was observed in the case of implantation-formed GaN:Er LEDs where biases in excess of 100V were used to produce 1.54 μm EL intensities comparable to PL intensities. Also, the relatively high-resistivity p-Si substrate (~ 10 Ω-cm) and the undoped GaN and AlN buffer layers probably contribute significant series resistance to the overall voltage drop through the device. Ideally, the optically active regions of an electroluminescent GaN:Er device would be in

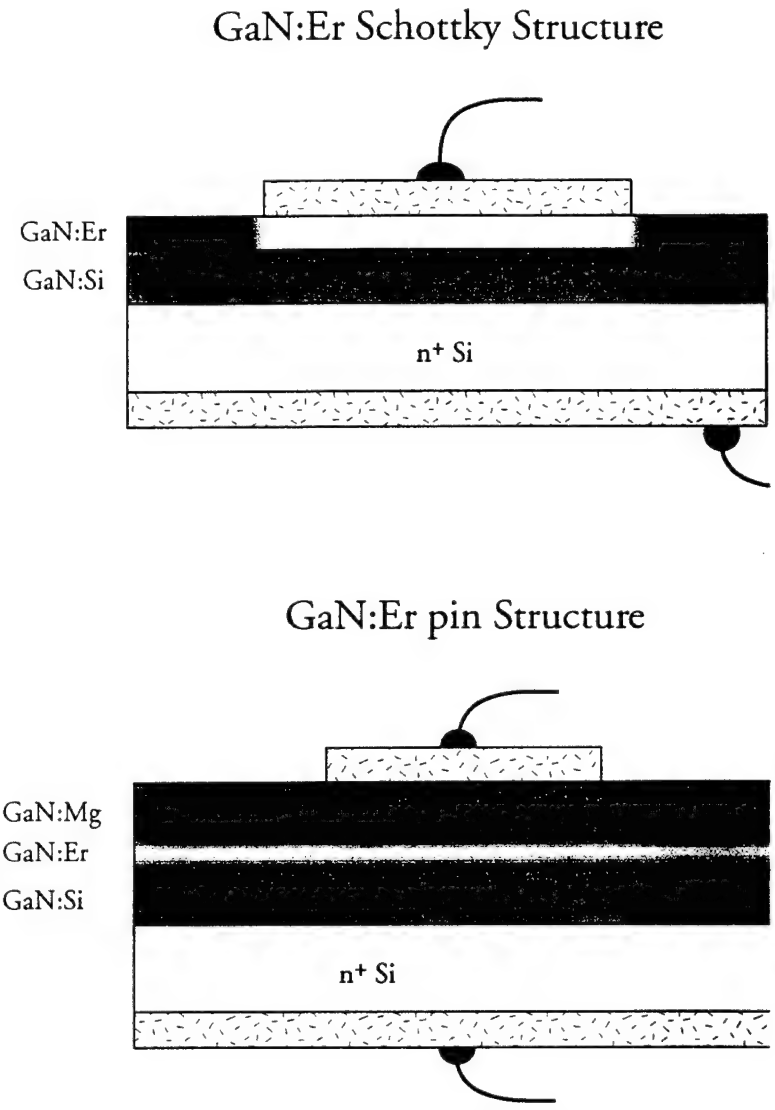

Figure 19. Cross-section diagrams of GaN:Er/GaN:Si/n^+Si Schottky (top) and GaN:Mg/GaN:Er/GaN:Si/n^+ Si p-i-n (bottom) diode structures.

contact with conductive injection layers such as in the n-Schottky and p-i(Er)-n structures shown in Figure 19 grown on low-resistivity Si.

However, growing such structures with plasma-assisted MOMBE presents a challenge in terms of impurity distributions. While the presence of high concentrations of carbon and oxygen from the metalorganic precursor are important for the optical activation of Er^{3+}, the presence of these impurities is also known to passivate electrical dopants in GaN. For example, magnesium, the most common p-type dopant currently used in GaN, is known to have a high affinity for oxygen. Attempts to produce p-type triethylgallium-derived GaN:Mg using bis-(cyclopentadienyl) magnesium and n-type GaN:Si using $SiBr_4$ with plasma-assisted MOMBE have not been successful. However, n-type (10^{19} cm^{-3}) and p-type (10^{16} cm^{-3}) GaN has been attained using 8N purity solid Ga metal evaporated from an effusion cell at approximately 950°C as the Group III source. In order to produce p-i(Er)-n and n-Schottky structures like those depicted in Figure 19, that would be both optically and electrically active, triethylgallium was used as the Group III source during the growth of the insulating, Er-containing layers and solid Ga was used during the deposition of n- or p-type injection layers. The magnesium, erbium and silicon profiles, as determined by SIMS are shown in Figure 20. The strongly-luminescent TEGa-derived GaN:Er films that produced the strong room-temperature PL depicted in Figure 17 had carbon and oxygen backgrounds of 10^{21} cm^{-3} and 10^{20} cm^{-3}, respectively. However, SIMS indicates that the C and O concentration in the TEGa-derived GaN:Er layer of the p-i-n structure are 2 x 10^{19} cm^{-3} and 2 x 10^{18} cm^{-3}, respectively. The Er^{3+} PL from this p-i-n structure is also significantly less intense than that observed from the TEGa-derived films grown previously. This variability in impurity background is likely due to the volatility of the ether in the TEGa source causing the ether to distill out over time. This results in a drop in the ether-associated impurity concentrations in TEGa-derived GaN over the lifetime of the TEGa bubbler charge.

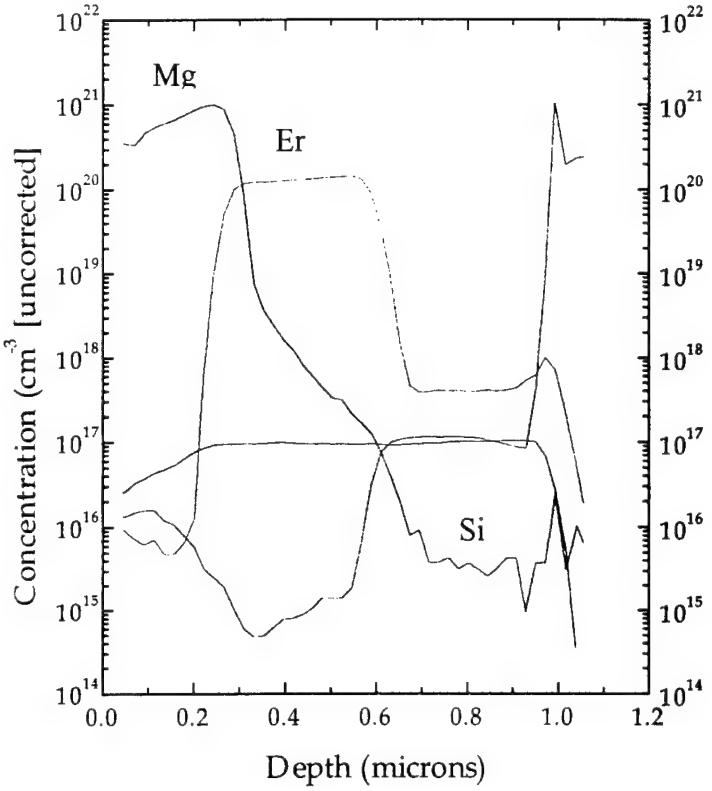

Figure 20. Secondary ion mass spectrometry profiles of the Mg-, Er-, and Si-doped layers of an MOMBE-derived p-i-n structure. Concentrations have not been corrected for sensitivity factor differences.

To further elucidate the impact of C and O on Er^{3+} activation, ion-implantation was used to introduce C and O into the p(Mg)-i(Er)-n(Si) structure grown on n^+-Si depicted in Figure 20. A 2 x 10^{15} cm^{-3} dose of carbon was implanted into the p-i-n structure at 200 keV to create a

carbon profile with a peak concentration of ~10^{20} cm^{-3} at a depth that coincided with the Er-doped layer. A second piece of the p(Mg)-i(Er)-n(Si) sample was implanted with a 2 x 10^{15} cm^{-3} dose of oxygen at 250 keV to create an oxygen profile with a peak concentration of ~10^{20} cm^{-3} centered at approximately the same depth as the Er-doped layer. The carbon and oxygen implant parameters were arrived at through iterative implant simulations using an Implant Sciences software package. These simulated implant profiles are shown in Figure 21. After implantation, the room-temperature Er^{3+} PL from the p-i-n structure was dramatically attenuated indicating that implantation damage produces a high concentration of states that compete non-radiatively with or channel energy out of the Er ion. Upon annealing at 625°C the Er^{3+} signal returned in both the carbon- and oxygen-implanted samples. As shown in Figure 22, after 930 seconds of annealing, the 1.54 μm signal in both the C- and O-implanted samples increased beyond the intensity measured for unimplanted samples, either unannealed or annealed. Carbon implantation induced a larger increase in Er^{3+} activation than oxygen implantation. This follows the results seen for Si:Er co-implantation by Michel et. al. [11]

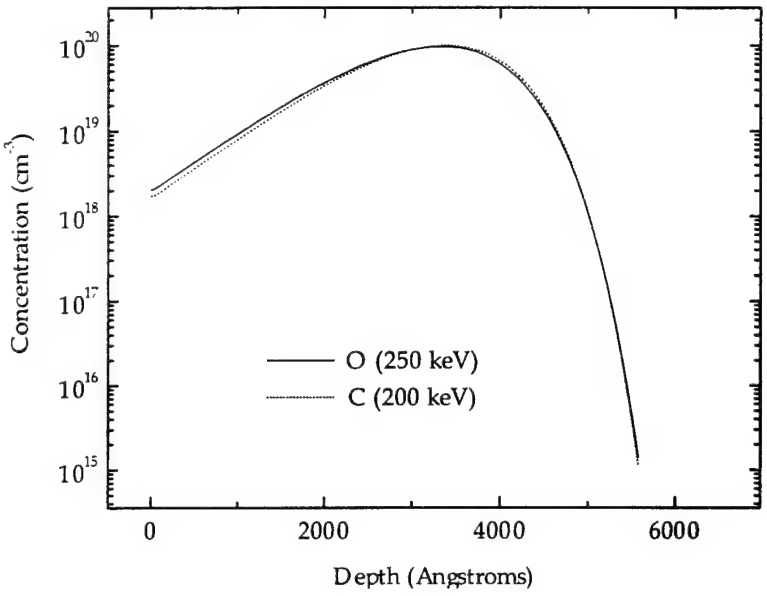

Figure 21. Computer simulations of a 250 keV oxygen implant and a 200 keV carbon implant into GaN.

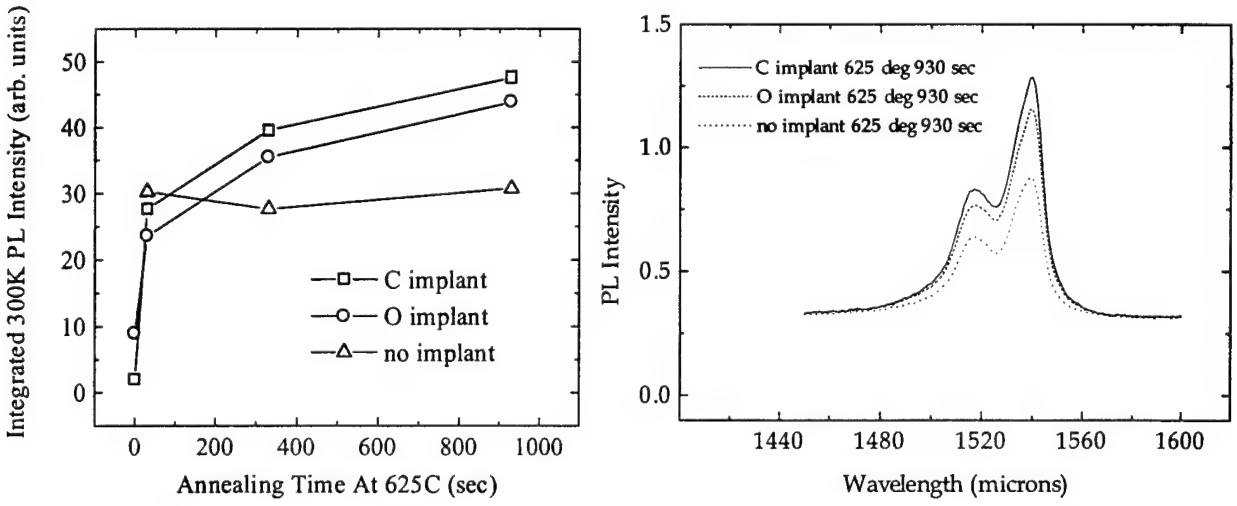

Figure 22. Effect of 625°C rapid-thermal-annealing on the Er^{+3} PL from O- and C-implanted GaN:Er p(Mg)-i(Er)-n(Si) structures. The figure at left compares the spectra of implanted and unimplanted samples after annealing. The plot at right shows the integrated 1.54 μm PL intensity as a function of annealing time for unimplanted and implanted samples.

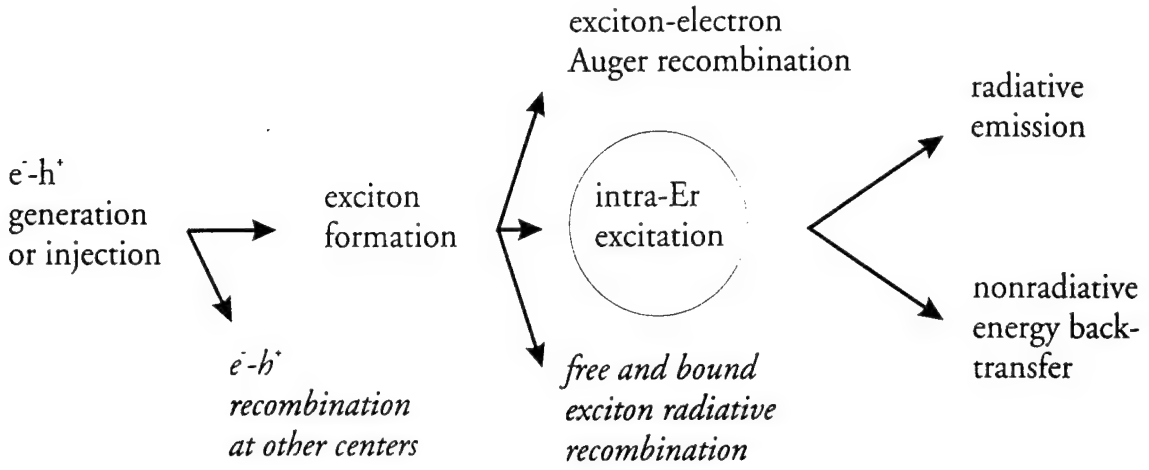

Figure 23. Energy flow diagram of Er^{3+} excitation proposed for Si:Er.[17,18]

Exciton-based energy transfer models have been proposed for excitations in Si:Er [15] and GaP:Er.[16] In the Si:Er model, intra-Er Auger excitation from excitons is mediated by a gateway state in the gap. This mechanism, including other radiative and non-radiative pathways, is illustrated in Figure 23. This model assumes that some mid-gap level exists at an energy conducive to transferring energy directly to the 4f levels of Er^{3+}. The existence of such a level also suggests the possibility of back-transfer processes where excited Er complexes could transfer an excited carrier back to this mid gap state which is subsequently thermalized up into the conduction band, effectively deactivating the erbium center. This model may be relevant to the GaN:Er luminescence mechanism observed in this study as the importance of carbon and oxygen co-doping have been well established. The fact that carbon has a greater impact on Er^{+3} luminescence efficiency than the more electronegative oxygen implies that ionic field effects are not of primary importance. Rather, it may be the introduction of beneficial mid-gap states that provide efficient energy transfer pathways for Er in GaN.

The effect of energy gap relative to the Er^{+3} pump levels on 1.54 μm PL efficiency was investigated in $In_{1-x}Ga_xAs_yP_{1-y}$ indicating that indirect energy transfer processes dominate rare-earth excitation in this material. [17] A diagram of this excitation model is shown in Figure 24. Only after the band energy was increased to 70 meV greater than the Er ($^4I_{11/2}$ - ground state) energy did the photoluminescence efficiency increase substantially. This strongly suggests that carrier/exciton-trapping, associated with a Coulombic field or a deformation potential around the substitutional Er ion, controls energy

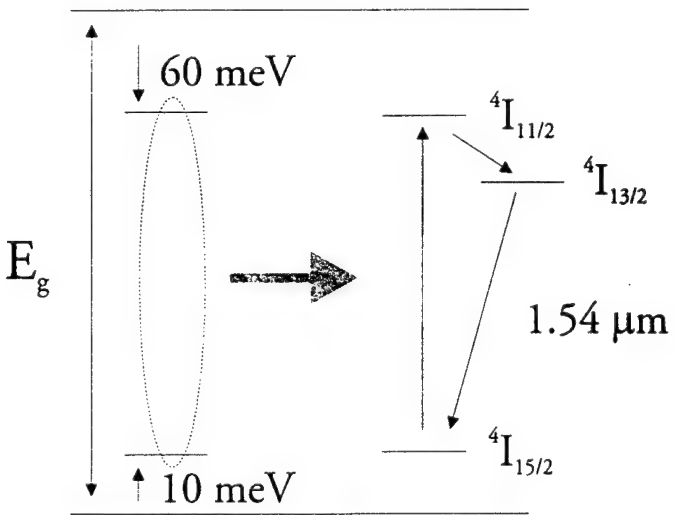

Figure 24. Energy diagram of exciton-trapping and energy transfer to the 4f levels of the Er^{3+} ion as proposed by Wellman et al.[17]

transfer to Er^{+3}. In rare earth-doped II-IV semiconductors, donor-acceptor pairs (DAPs) are believed to play the dominant role in excitation through localization of excitons.[18] Cathodoluminescence and PL results indicated a strong energy coupling from excited DAPs to the 4f levels of closely-associated rare-earth ions.[19] A component of the DAP may act as activator and sensitizer, such as an acceptor that provides a recombination trap pathway and compensates rare-earth ion charge. This may be particularly relevant to MOMBE-derived GaN:Er. The strongest 1.54 μm PL was observed for GaN:Er with high [C] and [O] backgrounds. Previously, carbon has been demonstrated to act as a heavily self-compensating acceptor in GaN.[20] Also, in the implantation experiments outlined earlier in this chapter, carbon was seen to have a greater impact on solid source-derived erbium activation than oxygen. Combining the models outlined in Figure 23 and 24, luminescence enhancement of GaN:Er may result from the introduction of charge-compensating acceptor-like states that provide energy transfer pathways for the excitation and de-excitation of MOMBE-derived GaN:Er. This model is further reinforced by initial experiments conducted with n-type InAlN:Er, which is characterized by high carbon backgrounds associated with the use of TMIn, and the observation of temperature-dependent 1.54 μm photoluminescence lifetimes for high [C] and [O] GaN:Er. Preliminary studies of Er^{3+} PL intensity as a function of InN mole fraction in $In_xAl_{1-x}N$:Er ternaries indicate that the onset of n-type conductivity may suppress Er^{3+} optical activation.

Beneficial effects of light-element co-doping have also been seen in the electroluminescence efficiency of Er in semiconductor hosts.[21] Since erbium excitations act within the parity-forbidden transitions allowed by weak field splitting in the 4f shell, the electric dipole interaction and therefore the electrical impact excitation cross-section of isolated Er ions is quite small. In isolation, the weakly-allowed intra-4f shell erbium transitions, induced by crystal field splitting are expected to have relatively long luminescence lifetimes such as the millisecond-regime lifetimes observed for Er in a number of hosts.[22] Complexing Er with electronegative codopants has been shown to enhance Er^{3+} electroluminescence intensity and reduce thermal quenching. This suggests that the impact excitation cross-section for rare-earth complexes and clusters is considerably larger than that of Er alone. This may explain why the high [C] and [O] structure depicted in Figure 16 exhibited electroluminescence in spite of the high series resistance, while no electrically-stimulated 1.54 μm signal was detected from the p-i(Er)-n structure. Photoluminescence lifetimes of TEGa-derived GaN were observed to be quite short, on the order of 100 microseconds. Also, the 1.54 μm PL lifetimes decreased with increasing temperature as shown in Figure 25. This coincides with the expected luminescence behavior for the mid-gap state-mediated excitation model depicted in Figure 23. In this case the probability of phonon-assisted thermalization of electrons out of the mid-gap state, back-transferring energy from the Er^{3+} ion, would increase with temperature following the increase in phonons available to induce such a transition. As the binding energy of these states increase, larger numbers of thermal phonons would be required to de-trap a carrier. Such a back-transfer process would deactivate excited Er ions, quenching radiative recombination and shortening the luminescence lifetime in agreement with the observed thermal PL quenching and lifetime behavior for MOMBE-derived GaN:Er.

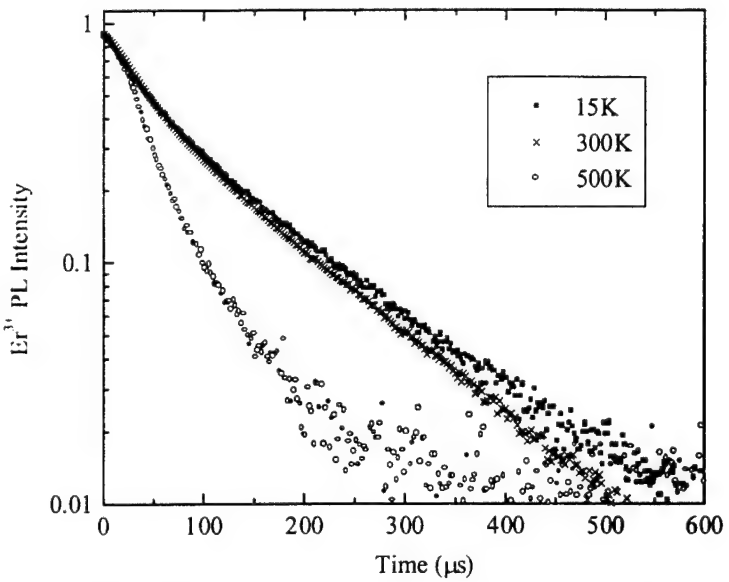

Figure 25. Photoluminescence decay curves (1.54 μm transition) for TEGa-derived GaN:Er at 15K, 300K and 500K.

Closer study of the temperature-dependence of the 1.54 μm luminescence lifetime further indicates that co-dopant related transfer states are involved in Er^{3+} excitation in MOMBE-derived GaN:Er. Photoluminescence lifetime and integrated intensity of the 1.54 μm Er^{3+} transition are plotted as a function of temperature for high [C] and [O] GaN:Er in Figure 26. Of immediate interest is the functional similarity between the lifetime and integrated intensity, both of which show a maximum near 200 K. As mentioned in the previous paragraph, the 100 microsecond-regime lifetimes are quite short. In Er-doped silica, increases in the fraction of excited Er ions are usually associated with shorter lifetimes.[12] These shorter lifetimes can be attributed to Er-Er interactions, such as cooperative upconversion in which the relaxation of an excited erbium ion directly stimulates another closely associated, excited erbium ion, putting it into a higher energy state which may then relax non-radiatively. This process ultimately leads to the quenching of 1.54 μm radiative emission. An example of this de-excitation process is shown inFigure 27. For GaN:Er the opposite behavior was observed. Near 200K, the increase in 1.54 μm luminescence lifetimes is associated with a corresponding increase in integrated intensity for sub-gap optical pumping. This suggests a thermally-activated state contributes to an increase in the $^4I_{13/2}$ - $^4I_{15/2}$ radiative lifetime. It is proposed that impurity states, associated with carbon, prohibit Er-Er de-excitation interactions and Er back-transfer mechanisms by strongly-trapping excitons and shielding long-range Er ion interactions through localization, and charge compensation. This accounts for the correlation of luminescence lifetime with intensity in TEGa-derived GaN:Er, the growth and implantation results seen previously in this work, and the models for trap- or mid-gap state-mediated Er energy back-transfer processes proposed for other semiconductor:Er systems.

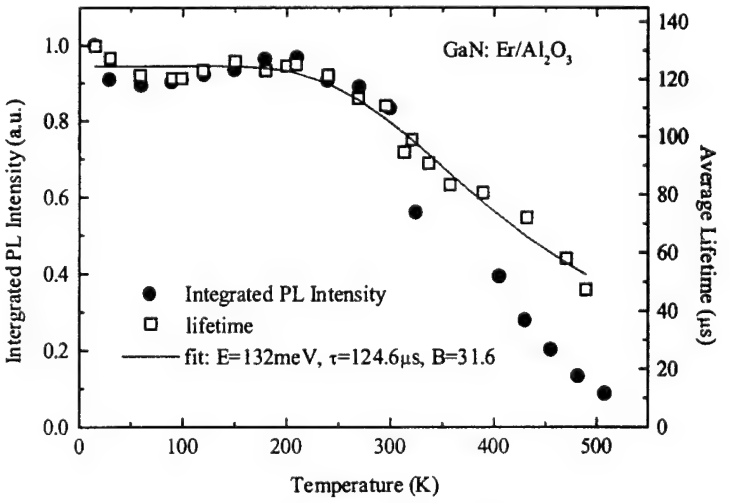

Figure 26. Photoluminescence lifetime (1.54 μm transition) and intensity as a function of temperature for TEGa-derived GaN:Er.

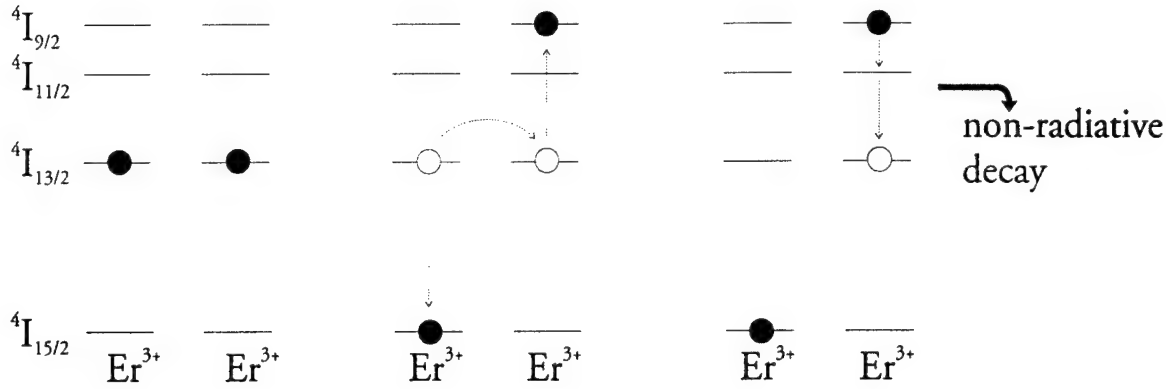

Figure 27. Energy diagram representing the successive configurations of closely associated Er^{3+} ions during upconversion de-excitation.

Low temperature cathodoluminescence (CL) spectroscopy of MOMBE-derived GaN:Er was performed by L. J. Brillson and his group at the Ohio State University.[23] Depth-dependent probing of the GaN:Er film with CL showed strong 0.8 eV emission (1554 nm) that corresponded to the Er doping profile. However, the profile of emission lines at 1.8 eV, 2.2 eV, and 2.3 eV, corresponding to other intra-4f shell Er^{3+} transitions[14] showed a noticeable interaction with near-surface defects that evolved with annealing;. Broadband sub-gap emission features, such as 'yellow' luminescence near 2.2 eV were not detected. Also, increases in 1.54μm Er^{3+} luminescence coincided with a decrease in the band-edge emission intensity. This suggests, in agreement with the photoluminescence lifetimes and impurity enhancement model proposed in this work, that the GaN:Er radiative process is fast and efficient, competing with band edge emission.

2.4 Eu Doping

Films were grown by GSMBE in a modified Varian INTEVAC Gas Source Gen II on In-mounted (0001) Al_2O_3. A high temperature surface nitridation preceded all layer growth, and was performed at a temperature of 865°C. A 10 nm low temperature AlN buffer layer (T_g = 435°C) was then grown using dimethylethylamine alane (DMEAA) as the aluminum source. This was followed by a 1.2 μm GaN:Eu layer grown at a temperature of 750°C. Solid source effusion cells provided the gallium (7N) and europium (4N) fluxes. Reactive nitrogen for the nitridation and for the growth of both the AlN and GaN layers was provided by an SVT RF plasma source operating at 375 W of forward power and 3 sccm of N_2. The shuttered europium cell was maintained at a temperature of 500°C. The GaN:Eu growth rate was ~92 Å/min. The room temperature Eu^{+3} photoluminescence (PL) was excited using the the 325 nm line of a HeCd laser while the AlGaAs was excited using the 514.5 nm line of an Ar ion laser. Emission for both materials was measured with a GaAs photomultiplier.

The results of PL analysis of the GaN:Eu film using above bandgap excitation from the HeCd laser are presented in Figure 28. The Eu^{+3} transition at 621 nm is due to the $^5D_0 \rightarrow {}^7F_2$ transition of the 4f shell. Also superimposed with the GaN:Eu spectra are spectra from both $Al_{0.35}Ga_{0.65}As$ and $Al_{0.30}Ga_{0.70}As$ using above bandgap excitation from the Ar ion laser. The laser power in both cases was approximately 35 mW. The emission from the GaN:Eu sample

was visible with the naked eye. From the figure, the GaN:Eu emission is more intense than both AlGaAs samples and also has a much narrower full width half maximum (FWHM). The FWHM of the GaN:Eu is approximately 2.2 nm, compared to 14 nm for the $Al_{0.35}Ga_{0.65}As$, and 13 nm for the $Al_{0.30}Ga_{0.70}As$. Rapid thermal annealing results for both N_2 and forming gas (10% H_2/90% N_2) ambients are presented in Figure 29. After annealing at 800 °C, the integrated PL for both cases is virtually identical to the as grown values. The increased emission after annealing at 400°C and 600°C may be due to the enhanced promotion of Eu from the +2 state to the +3 state and also to the removal of nonradiative defect sites. The decrease in emission after annealing at 800°C may be due to the precipitation of separate Eu phases from GaN:Eu solid solution.

Thermal quenching measurements (Figures 30 and 31) on both the as-grown and 800°C N_2 annealed samples were performed with a liquid He cooled coldfinger. The as grown sample was found to quench by approximately 82% as the measurement temperature was increased from 20K to 300K. After annealing in N_2, the thermal quenching was reduced to 66% over the same measurement range. The improved quenching behavior further verifies the conclusion from Figure 29 that the improvement in emission upon annealing is due to the removal of nonradiative defects and the enhancement of the Eu from the +2 to the +3 valence state. At low temperatures, additional peaks were visible at 598 nm, 606 nm, 616 nm, and 632 nm as shown in Figure 31.

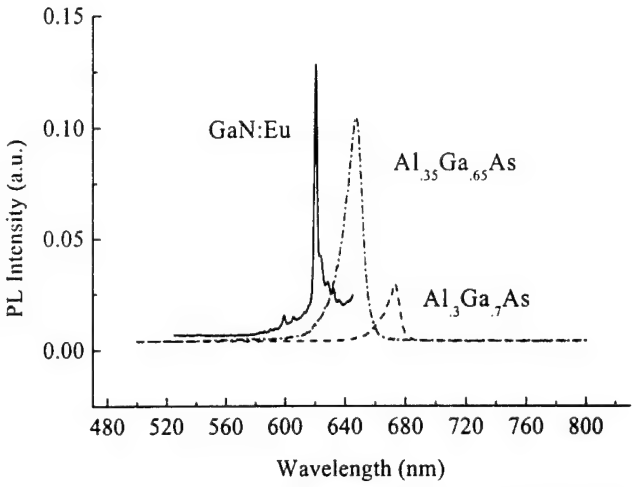

Figure 28. PL spectra of GaN:Eu in comparison with MOCVD derived AlGaAs.

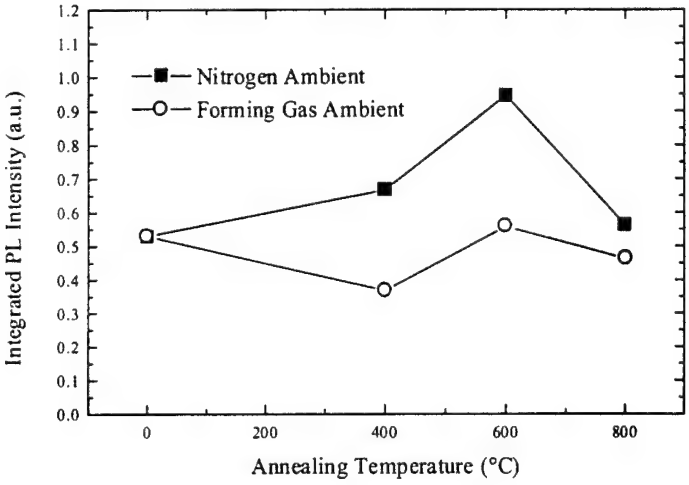

Figure 29. Integrated 621 nm PL intensity for GaN:Eu annealed in either N_2 or forming gas ambient.

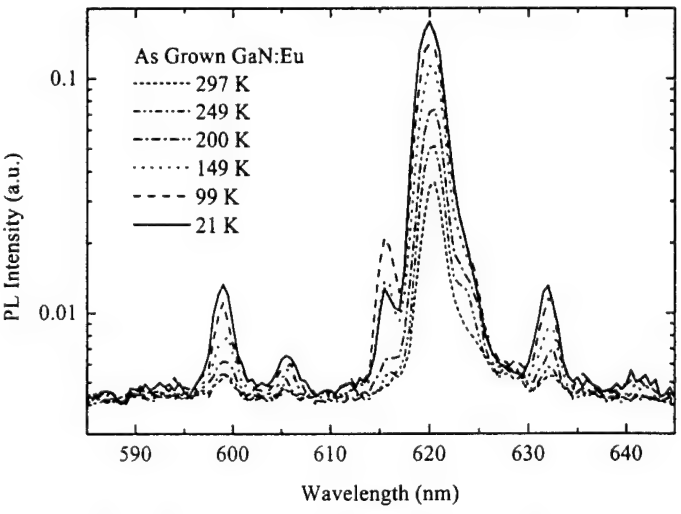

Figure 30. PL spectra taken at various measurement temperatures from as-grown GaN:Eu.

The surface morphology of the GaN:Eu did not change significantly after annealing. AFM scans of the as grown GaN:Eu and the material annealed at 800°C in N_2 is given in Figure 32. The measured root mean square (RMS) surface roughness increased slightly from 17.5 nm to 17.9 nm, suggesting that annealing has not caused significant precipitation of a second phase within the GaN:Eu. However, further analysis is needed to confirm the absence of precipitation.

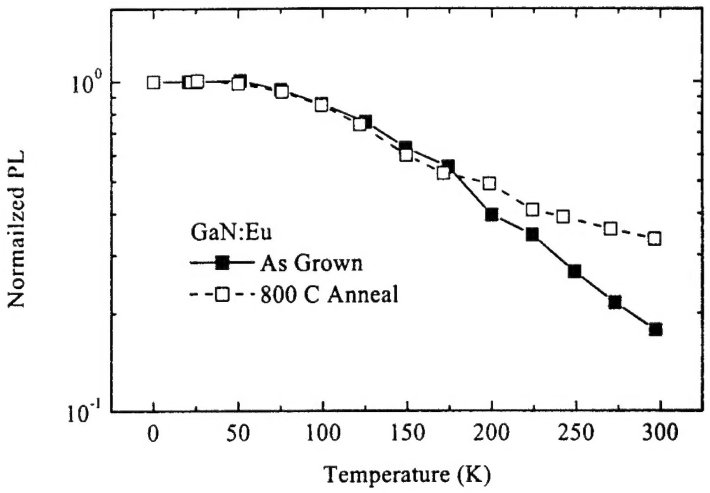

Figure 31. Thermal quenching results for both as grown and N_2 annealed GaN:Eu.

3.0 CONCLUSIONS

Under this program it was shown that GaN:Er does not exhibit the same type of surface roughening with increasing Er content that is observed for AlN. Surface morphologies and surface roughness actually improved with Er flux due to a reduction in the column size and shape. Also unlike AlN:Er, the integrated 1.54 μm PL intensity did not saturate with Er flux, but rather increased even at high Er fluxes. It was also shown that codoping of GaN:Er with C can be beneficial. The integrated 1.54 μm PL intensity reaches a maximum for an optimum C concentration, similar to work done with Si:Er:O. This indicates Er-C complex formation initially increases the PL, but further codoping creates defects that enhance nonradiative recombination. Some of these defects can apparently be removed by high temperature annealing. Comparison of the quenching behavior of GaN:Er,C grown using elemental Ga and CBr_4 with GaN:Er,C,O grown using TEG suggests that oxygen is more effective at suppressing thermal quenching than carbon.

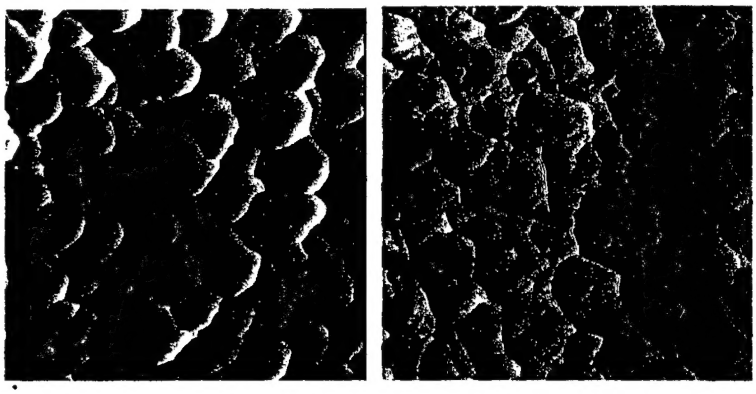

Figure 32. 1 μm x 1 μm AFM scans of as grown GaN:Eu (left) and GaN:Eu annealed at 800 °C in N_2 (right).

Electroluminescence from GaN and InAlN doped with erbium during growth by plasma-assisted MOMBE was also demonstrated. For the first time, the integration of GaN:Er and InAlN:Er with silicon in devices operating at room temperature has demonstrated the feasibility for III-N:Er near-IR optoelectronics. Explicit studies have further verified the beneficial impact of light impurities on GaN:Er luminescence and electroluminescence. These results, and the photoluminescence and cathodoluminescence behavior of MOMBE-derived GaN:Er suggest that a thermally activated, acceptor-like state associated with carbon which inhibits Er de-excitation.

Finally, visible red emission at 621 nm from GaN:Eu grown by GSMBE was observed. The emission was found to be more intense than that obtained from MOCVD AlGaAs excited with an Ar+ laser. Annealing up to 800 °C in either N_2 or forming gas did not significantly change the PL or the surface morphology, but did slightly reduce the degree of thermal quenching. This suggests that the reduction in thermal quenching is due to the removal of nonradiative defects within the GaN:Eu material and to the promotion of the Eu from the +2 to the +3 state.

4.0 REFERENCES

[1] K. Okada, Y.-F. Wang, and T. Nakaya, *Synthetic Metals*, **97**, 113 (1998).

[2] D. Rüter and W. Bauhofer, *Appl. Phys. Lett.*, **69**, 892 (1996).

[3] T. Chatterjee, P. J. McCann, X. M. Fang, and M. B. Johnson, *J. Vac. Sci. Technol. B*, **16,** 1463 (1998).

[4] J. Heikenfeld, M. Garter, D. S. Lee, R. Birkhahn, and A. J. Steckl, *Appl. Phys. Lett.*, **75,** 1189 (1999).

[5] D. S. Lee, J. Heikenfeld, R. Birkhahn, M. Garter, B. K. Lee, and A. J. Steckl, *Appl. Phys. Lett.*, **76**, 1525 (2000).

[6] F. Priolo, S. Coffa, G. Franzó, C. Spinella, A. Carnera, and V. Bellani, J. Appl. Phys. **74,** 4936 (1993).

[7] S. Coffa, F. Priolo, G. Franzó, A. Polman, S. Libertino, M. Saggio, and A. Carnera, Nucl. Instr. and Meth. in Phys. Res. B **106**, 386 (1995).

[8] Priolo, S. Coffa, G. Franzó, C. Spinella, A. Carnera, and V. Bellani, J. Appl. Phys. **74,** 4936 (1993).

[9] M. Markmann, E. Neufeld, A. Sticht, K. Brunner, G. Abstreiter, and Ch. Buchal, Appl. Phys. Lett. **75**, 2584 (1999).

[10] F. Priolo, G. Franzó, S. Coffa, A. Polman, S. Libertino, R. Barklie, and D. Carey, J. Appl. Phys. **78,** 3874 (1995).

[11] J. Michel, J. L. Benton, R. F. Ferrante, D. C. Jacobson, D. J. Eaglesham, E. A. Fitzgerald, Y. -H. Xie, J. M. Poate, and L. C. Kimmerling, *J. Appl. Phys.*, **70** (1991) 2672.

[12] A. Cros., H. Angerer, R. Handschuh, O. Ambacher and M. Stutzmann, *Mat. Res. Soc. J. Nitr. Sem. Res.*, **2** (1997) 43.

[13] S. Lombardo, S. U. Campisano, G. N. van den Hoven and A. Polman, *Appl. Phys. Lett.*, **77** (1995) 6504.

[14] J. Torvik, R. J. Feuerstein, J. I. Pankove, C. H. Qiu, and F. Namavar, *Appl. Phys. Lett.* **69** (1996) 2098.

[15] J. Michel, B. Zheng, J. Palm, E. Oullette, F. Gan, and L. C. Kimmerling, *Mat. Res. Soc. Proc.*, **422** (1996) 317.

[16] X. Z. Wang and B. W. Wessels, *Appl. Phys. Lett.*, **64** (1994) 1537.

[17] P. Wellman, A Winnacker, and G Pensl, *Mat. Res. Soc. Proc.*, **422**, (1996) 255.

[18] M. Godlewski, *Mat. Res. Soc. Symp. Proc.*, **422** (1996) 291.

[19] D. Hommel, W. Busse, H.-E. Gumlich, D. Suisky, J. Rosler, K. Swiatek, and M. Godlewski, J. Cryst. Growth, **101** (1990) 393.

[20] C. R. Abernathy, J. D. MacKenzie, S. J. Pearton, W. S. Hobson, *Appl. Phys. Lett.*, **66** (1995) 1969.

[21] G. Franzo, F. Priolo, S. Coffa, A. Polman, and A Carnera, *Nucl. Instr. and Meth. in Phys. Res. B*, **96** (1995) 374.

[22] J. M. Zavada and D. Zhang, *Sol. State Elec.*, **38** (1995) 1285.

[23] T. Levin, I. Shafer, A. P. Young, L. J. Brillson, J. D. MacKenzie, and C. R. Abernathy, Presented at the Amer. Vac. Soc. 45th Int. Symp., Baltimore, Nov. 1998.

[24] M. Thaik, U. Hommerich, R. N. Schwartz, R. G. Wilson and J. M. Zavada, *Appl. Phys. Lett.*, **71** (1997) 2641.

5.0 PUBLICATIONS RESULTING FROM THIS PROGRAM

1. "Er Doping of GaN During Growth by Metalorganic Molecular Beam Epitaxy," J. Devin MacKenzie, C.R. Abernathy, S.J. Pearton, Appl. Phys. Lett., June 25, 1998.

2. "Luminescence Enhancement in AlN(Er) by Hydrogenation," S.J. Pearton, C.R. Abernathy, J.D. MacKenzie, R.G. Wilson, R.N. Schwartz and J.M. Zavada, Appl. Phys. Lett. 71, 1807 (1997).

3. "Effect of Atomic H on Er Luminescence from AlN," S.J. Pearton, C.R. Abernathy, J.D. MacKenzie, U. Hommerich, J.M. Zavada, R.G. Wilson and R.N. Schwartz, J. Vac. Sci. Technol. A16, (1998).

4. "Novel Substrates for Growth of III-Nitrides", J. D. MacKenzie, S. M. Donovan, C. R. Abernathy, P. H. Holloway, R. M. Linares, B. Chai, J. Electrochem. Soc.

5. "Er Incorporation and Optical Activity in III-V Nitrides Grown by MOMBE," J. MacKenzie, C.R. Abernathy, S.J. Pearton, U. Hommerich, F. Ren, R.G. Wilson and J.M. Zavada, Fall Materials Research Society Meeting Proceedings Vol. 468, 123-129 (1997).

6. U. Hommerich, M. Thaik, R. N. Schwartz, R. G. Wilson, J. M. Zavada, S. J. Pearton, C. R. Abernathy and J. D. MacKenzie, *Electrochem. Soc. Proc.*, **98-2** (1998) 110.

7. "The Effect of Er Concentration on the Morphology and Photoluminescence of GaN:Er," M. E. Overberg, J. Brand, J. D. MacKenzie, C. R. Abernathy, S. J. Pearton and J. M. Zavada, J. of the Electrochem. Soc., **147**, 3117 (2000).

8. M. E. Overberg, J. Brand, J. D. MacKenzie, C. R. Abernathy, S. J. Pearton, and J. M.

Zavada, *Proc. of the State-of-the-Art Program on Comp. Semi. XXX,* Electrochem. Soc. Proc. **99-4**, 195-200 (1999).

9. "Photoluminescence Enhancement and Morphological Properties of Carbon Co-Doped GaN:Er," M. E. Overberg, C. R. Abernathy, S. J. Pearton, R. G. Wilson and J. M. Zavada, MRS Internet J. of Nitride Semicond. Res., 5S1, W11.62 (2000).

10. "Effect Of Carbon Doping On GaN:Er," Mark Overberg, Cammy R. Abernathy, J. Devin MacKenzie, Stephen J. Pearton, Robert G. Wilson and John M. Zavada, Materials Science and Engineering: B 81 (1-3) (2001) pp. 121 - 126.

11. "Eu Doping Of GaN," Mark Overberg, K. N. Lee, Cammy R. Abernathy, Stephen J. Pearton, Robert G. Wilson and John M. Zavada, Materials Science and Engineering: B 81 (1-3) (2001) pp. 150 - 152.

12. "Localized states at GaN surfaces, Schottky barriers, and quantum well interfaces," L.J. Brillson, A.P. Young, T.M. Levin, G.H. Jessen, J. Schäfer, Y. Yang, S.H. Xu, H. Cruguel, G.J. Lapeyre, F.A. Ponce, Y. Naoi, C. Tu, J.D. McKenzie, C.R. Abernathy, Materials Science and Engineering: B 75 (2-3) (2000) pp. 218 - 223.

13. "Spectroscopic studies of the visible and infrared luminescence from Er doped GaN," U. Hömmerich," J.T. Seo, C.R. Abernathy, A.J. Steckl, J.M. Zavada, Materials Science and Engineering: B 81 (1-3) (2001) pp. 116 - 120.